The Lower Main Sequence and the Orbital Period Distribution of Cataclysmic Variable Stars

J. Christopher Clemens

I. Neill Reid [1]

John E. Gizis

Palomar Observatory, 105-24, California Institute of Technology, Pasadena, CA 91125, e-mail: jcc@astro.caltech.edu, inr@astro.caltech.edu, jeg@astro.caltech.edu

M. Sean O'Brien

Department of Physics and Astronomy, Iowa State University, Ames, IA 50011, e-mail:msobrien@iastate.edu

ABSTRACT

The color-magnitude diagram of the lower main sequence, as measured from a volume-limited sample of nearby stars, shows an abrupt downward jump between $M_V \sim 12$ and 13. This jump indicates that the observed mass-radius relationship steepens between 0.3 and 0.2 $M_\odot$, but theoretical models show no such effect. It is difficult to isolate the source of this disagreement: the observational mass-radius relationship relies upon transformations that may not be sufficiently accurate, while the theoretical relationship relies upon stellar models that may not be sufficiently complete, particularly in their treatment of the complex physics governing the interior equation-of-state.

If the features in the observationally derived mass-radius relationship are real, their existence provides a natural explanation for the well-known gap in the orbital period distribution of cataclysmic variables. This explanation relies only upon the observed mass-radius relationship of low-mass stars, and does not require *ad hoc* changes in magnetic braking or in the structure of cataclysmic variable secondaries. If correct, it will allow broader application of cataclysmic variable observations to problems of basic stellar physics.

Subject headings: stars: late type — cataclysmic variables

[1] Visiting Research Associate, Observatories of the Carnegie Institution of Washington

1. Introduction

As physics laboratories, stars leave something to be desired. The number of observable stellar parameters is usually far outmatched by the number of unknowns contained in a stellar model. To progress, theorists must eliminate variables through the use of relations based on the best possible constitutive physics. When, inevitably, the resulting models fail to match all the observational details, it is difficult to know which physics to adjust. This is unfortunate, because it is precisely in the mismatch between theory and observation that the opportunity to improve physical insight lies.

The best solution to this dilemma is to increase the number and variety of observational constraints. Many interesting experiments, not of our design, make this possible. For stellar astronomers, the most dramatic, and potentially revealing, are those offered by interacting binary stars, particularly the cataclysmic variable stars. These are binaries consisting of a low-mass secondary (typically $< 1\mathrm{M}_\odot$) transferring matter, usually through an accretion disk, onto a white dwarf star. Warner (1995; see also Patterson 1984), has written an excellent and comprehensive review of these systems.

The secondaries in cataclysmic variables, which are being slowly stripped of mass, offer a perspective on the lower main sequence not available from single low-mass stars, which spend their entire lives at more-or-less constant mass. Unfortunately, the complexities of the mass transfer introduce a spectacular, often bewildering array of observational properties that must be interpreted with caution. These include complex geometric modulations, rapid photometric flickering, and outbursts with amplitudes up to 19 magnitudes. Fortunately, it is usually possible to measure at least one parameter, the orbital period, with high accuracy.

In this paper, we will explore the connection between cataclysmic variable orbital periods and observations of low-mass single stars, under the simplest of assumptions. In particular, we will examine a downward jump that appears around $M_V \sim 12$ in color-magnitude diagrams of population I stars. The location of this jump, and its effect on the inferred mass-radius relationship, provide a reasonable and natural explanation for the most distinctive feature of the cataclysmic variable orbital period distribution, the period gap.

2. The Lower Main Sequence

In this section, we will examine the morphology of the lower main sequence using color-magnitude diagrams of a volume-limited sample of nearby stars defined by Reid & Gizis (1997). The ultimate purpose of this exploration is to show that the observations

contain evidence for changes in the slope of the mass-radius relationship—changes not reproduced by theoretical models of low-mass stars. To construct the mass-radius diagram, we will transform the observations into the theoretical plane using the best available bolometric corrections and effective temperature scale (Leggett et al. 1996). Then we will investigate the implied shape of the mass-radius relationship using the empirical mass-magnitude relationships of Henry & McCarthy (1993). The most uncertain component of this process, and the only one which depends explicitly upon theoretical models, is the color-temperature transformation. Consequently, we will discuss in detail whether the discrepancy between theory and observation results from this problematic transformation, or whether it arises from inadequacies in the stellar models.

2.1. The Observations

Reid, Hawley & Gizis (1995) have recently completed a spectroscopic survey of M-dwarfs drawn from the most recent version of the Catalogue of Nearby Stars (Gliese & Jahreiss 1991). In the course of this survey, Hawley, Gizis & Reid (1996) noted that the color-magnitude diagram of the stars with the best trigonometric parallaxes and photometric measurements shows a step or break near $(V-I) \sim 2.9$. This is apparently the same feature noted by Leggett, Harris, & Dahn (1994) in their observations of Hyades dwarfs. It also appears in published color-magnitude diagrams of NGC 2420 and NGC 2477, as measured with the *Hubble Space Telescope* by von Hippel et al. (1996).

Subsequent to the M-dwarf survey, Reid & Gizis (1997) showed that the survey stars north of $\delta = -30^o$ comprise a statistically complete sample to 10 parsecs for $M_V \leq +14$. Then they used the nearest 8 parsecs of the sample to study the fraction of multiple stars and its effect on the stellar luminosity function. In this paper we will use the same 8 parsec sample to examine the mass-radius relationship of stars on the lower main sequence. The details of this sample, along with a complete listing of the stars and their properties, can be found in Reid & Gizis (1997).

Our investigation does not strictly require a volume-limited sample, but the 8 parsec sample of Reid & Gizis (1997) offers two virtues: it was not selected on any subjective basis which might bias the shape of the color-magnitude diagram, and its $(M_V, (V-I))$ main sequence was fitted with a composite relation by Reid & Gizis (1997) before any of us recognized the connection to cataclysmic variables. We have used this fit, rather than calculating our own, so that there is no chance for bias to enter in the selection of fitting points.

The upper panels of Figure 1 show the $(M_V, (V-I))$ and $(M_K, (I-K))$ main sequences of stars from the 8 parsec sample. The photometry and distance determinations are compiled from a variety of published sources, as tabulated by Reid & Gizis (1997). The open circles denote stars for which the photometry is of lower quality, either because it was transformed from another photometric system into the Kron-Cousins system, or because the stars are components of small separation (< 5") binaries. For the solid points, Reid & Gizis (1997) note that the photometric accuracy in $(V-I)$ is 0.02 magnitudes, but the observed dispersion is 0.09, implying some intrinsic scatter in their properties. The average dispersion in M_V is ~ 0.35 magnitudes, but changes with the slope of the main sequence.

In the bottom panel of Figure 1, we have augmented the data with distances from Hipparcos (ESA 1997) to better define the main sequence above $M_V \sim 11$. This diagram shows intriguing suggestions of structure in the main sequence near $M_V \sim 8.5$, but unfortunately Hipparcos does not reach faint enough to help with the region of primary concern in this paper. Consequently, we have not used the Hipparcos data in any of the analysis which follows.

The step-like feature discussed by Hawley et al. (1996) appears in all three of the panels in Figure 1. In the $(M_V, (V-I))$ plot, we have added a dotted line representing the composite fit to the data by Reid & Gizis (1997). This fit maintains a roughly constant dispersion in $(V-I)$, and is described by the following formulae:

$$M_V = \begin{cases} 1.087 + 6.226(V-I) - 1.340(V-I)^2 + 0.187(V-I)^3 & \text{for } (V-I) < 2.635 \\ & (\sigma_V = 0.35 \text{ mag}) \\ 5.48(V-I) - 2.83 & \text{for } 2.635 \leq (V-I) < 3.00 \\ & (\sigma_V = 0.46 \text{ mag}) \\ 6.07 + 2.441(V-I) + 0.0233(V-I)^2 & \text{for } (V-I) \geq 3.00 \\ & (\sigma_V = 0.26 \text{ mag}) \end{cases} \tag{1}$$

2.2. Comparison to Theoretical Models

In order to compare the observations in Figure 1 to theoretical models, we have translated the data from color and magnitude to luminosity and temperature. The transformations we applied are based on the bolometric corrections and temperature scale

derived by Leggett et al. (1996), who used flux-calibrated spectra and trigonometric parallaxes to measure the bolometric correction for 16 M-dwarfs with colors in the range $1.56 < (V - I) < 4.26$.

To apply their measurements to the 8 parsec sample, we have fitted a parabola to their values of bolometric corrections and $(V - I)$ colors of the stars they identify as disk population. We find

$$BC_V = 0.477 - 0.765(V - I) - 0.099(V - I)^2, \tag{2}$$

where BC_V is the Johnson V band bolometric correction. We applied bolometric corrections calculated from this equation to the absolute V magnitudes of our sample and converted the result to $\log(L/L_\odot)$ using $M_{bol,\odot} = +4.75$.

Leggett et al. (1996) measured temperatures for their sample by fitting the observed spectra with improved versions of the atmospheric models of Allard & Hauschildt (1995). Again we fitted a parabola to their temperature measurements of disk stars to get the color-temperature relation:

$$T_{eff} = 5757.8 - 1218.6(V - I) + 116.9(V - I)^2. \tag{3}$$

In this instance we weighted our fit according to the published error estimates for the temperature values.

Our fitting formulae reproduce the measurements of Leggett et al. (1996) with a dispersion of 41 K in the temperature and 0.06 magnitudes in the bolometric correction. Leggett et al. estimate the errors in their temperatures to be 150-250 K.

The use of parabolic fits in both cases introduces implicit assumptions about the smoothness of the transformations, which are sparsely sampled by the Leggett et al. (1996) data. Considering the smoothness of similar, but better sampled transformations (Bessell 1995; Dahn et al. 1992) and of theoretically calculated ones (Allard & Hauschildt 1995; Brett 1995) these are probably safe assumptions, but we will return to this issue in Section 2.4.1.

In Figure 2, we plot the result of our transformations, along with a variety of stellar models. For clarity we have divided the models between 2 plots, both of which show the same observations. We have estimated the errors in temperature by propagating the dispersion in $V - I$, which overestimates the measurement error, through equation 3, and adding the dispersion in our temperature fit (in quadrature). We get 62-77 K, with the higher value applying to larger temperatures, where the $(T_{eff}, (V - I))$ relation is steeper. We estimated the luminosity errors in a similar manner using equation 2, but also included

the dispersion in M_V, which completely dominates the other terms. The error in $\log(L/L_\odot)$ ranges from 0.12 to 0.19, reflecting the changes in the σ_V of equation 1. For reference, both plots also show the composite relation of Reid & Gizis (1997) transformed in the same manner as the data.

It is encouraging that all of the models show a downturn more-or-less resembling the feature in the data. The atmosphere and envelope calculations in this temperature domain are notoriously difficult (Allard & Hauschildt 1995; Brett, 1995), and must incorporate the complex effects of molecule formation upon opacities (Alexander & Ferguson 1994) and the envelope equation-of-state (Saumon, Chabrier, & Van Horn 1995). It is a triumph that the models, particularly those of Baraffe et al. (1995) and Baraffe & Chabrier (1996) match the data so well. Nonetheless, the downward step in the data is more abrupt than that shown by any of the models. In the following section, we investigate the effect of this abruptness on the mass-radius relationship.

2.3. Implications for the Mass-Radius Relationship

The shape of the observed color-magnitude diagrams in Figures 1 and 2 implies that a rapid drop in stellar radius occurs between $M_V \sim 12$ and 13. To see whether it also implies a steepening of the mass-radius relationship, we have translated the data to the mass-radius plane using the same method as Hoxie (1973). First we used

$$R = (\frac{L}{4\pi\sigma})^{1/2} T^{-2}, \tag{4}$$

to calculate radii directly for the temperature and luminosities plotted in Figure 2. Then, to get masses, we used the empirical (mass, M_V) relation of Henry & McCarthy (1993), which is based on measurements for 37 stars in visual binaries. We chose the Henry & McCarthy relation because it is empirical, but the theoretical relations of Kroupa, Tout, & Gilmore (1993) and of Chabrier, Baraffe, & Plez (1996) yield similar results (shown in Figure 9).

Figure 3 shows the resulting mass-radius relationship. The lines and symbols are the same as in Figure 2, except here we show only the models of Baraffe & Chabrier (1996). We have placed representative error bars on the transformed fit of Reid & Gizis (1997). In the radius direction they represent the temperature and luminosity errors (described earlier) propagated through the radius calculation. In spite of the sensitivity of radius to temperature, the radius error is dominated by the scatter in M_V. Consequently, the error bars shown do not differ substantially from the scatter in the individual mass-radius points. Even if we increase the temperature error to 150 K, the estimate Leggett et al. (1996) give for most of their individual measurements, it does not significantly increase the radius error

we calculate. The mass error bars are the quadrature sum of the dispersion in the 8 parsec data M_V measurements and Henry & McCarthy's (1993) published dispersions for the (mass, M_V) relation. The latter are the largest contributors to the resultant error in mass.

Figure 3 illustrates the main point of this section: the mass-radius relationship of stars in the 8 parsec sample shows evidence for changes in slope not present in the theoretical models. The changes appear artificially abrupt in the dotted-line fit of Figure 3, reflecting the abrupt changes in the composite relations, both for $(M_V, (V-I))$, and for (mass, M_v). Otherwise, Figure 3 displays a realistic depiction of the empirical mass-radius relation of the 8 parsec sample, inclusive of any systematic errors in the photometry and transformations. We discuss the possible effects of these in the next section.

2.4. Discussion

The differences between the theoretical models and the transformed observations in Figure 3 are not large, but we will show in section 3 that their effect on the orbital period evolution of cataclysmic variables is profound. Consequently, it is important to establish how much faith ought to be placed in the observations and how much in the models. First, we will consider whether the slope changes in the observed mass-radius relationship might be generated as artifacts either from the photometric data or the transformations we have applied. We will not be able to completely exclude this possibility. Second, we will investigate the models and find that the physical parameters the modelers vary have substantial effects on the way model temperatures change with mass, but very little effect on the way model radii change with mass. As a result, the possibility of changes in the slope of the mass-radius relationship is not explicitly addressed by current models, and therefore cannot be ruled out.

2.4.1. The Observations and Transformations

Figure 4 illustrates two partially independent checks on the reality of the features in the mass-radius relationship of the 8 parsec sample. First, we have plotted the masses and radii of binaries tabulated by Popper (1980). With the exception of the eclipsing binaries CM Dra and YY Gem, the Popper data do not represent fundamental radius measurements. The radii were calculated via the same method we have used, but with different bolometric corrections and temperature transformations. The Popper data are consistent with the shape we have measured for the mass-radius relation, but contain too few fundamental

points to confirm the changes in slope. Furthermore, the most useful eclipsing system, CM Dra, is probably metal poor (Metcalfe et al. 1996; Gizis 1997), and inappropriate for comparison to our population I data.

For the second test illustrated in Figure 4, we have repeated the entire set of calculations required to generate our mass-radius relationship in a different photometric bandpass. This yields a separate measure of the observed mass-radius relationship, with independent photometric colors. First, we fitted the (BC_k, (I-K)) and (T_{eff}, (I-K)) data of Leggett and used these fits to transform the (M_k, (I-K)) data shown in the upper right panel of Figure 1. From this we constructed a mass-radius relation, this time using the (mass, M_k) relations of Henry & McCarthy (1993). This exercise does not address the question of systematic errors in the masses, temperatures or distances, which are common to both sets of transformations. The circles in Figure 4 show the final result. For reference, the dotted line is the same as in Figure 3. While the K-band mass-radius relation shows the same morphology as in the V-band, the slope changes are more muted, and the deviation from theoretical models smaller. These differences give us a feel for the size of systematic differences between the V and K band photometry and transformations, but they do not add any weight to the observed features in the mass-radius relationship.

In addition to the reality checks depicted in Figure 4, we have directly explored the possibility that errors in the transformations could generate artifacts in the mass-radius relation. For instance, the parameterized (mass, M_V) relation of Henry & McCarthy contains two inflection points as does the parameterized color-magnitude diagram from Reid and Gizis. We have tried moving these inflections points artificially to see if they can cancel to yield a mass-radius relation more like that of the theoretical models. This does not work very well: we must either move the inflection points so far that the fit to the slope of the (mass, M_V) data is unacceptably poor, or we must introduce a discontinuity in the mass-radius relation near 0.4 $R_\odot$. Furthermore, ten of the stars included in our mass-radius relation are from the Henry & McCarthy sample, and they show evidence for slope changes without recourse to the parameterized (mass, M_V) relation. Consequently it is unlikely that the observed slope changes are the result of systematic errors in the (mass, M_V) relation alone.

We have also experimented with the color-temperature transformation, which is the only transformation we have used that relies on theoretical models. We mentioned earlier that the shape of our transformations is not well sampled by the data of Leggett et al. (1996). Consequently we have experimented with changes required to transform the color-magnitude diagram into exact correspondence with the model of Baraffe & Chabrier (1996). Given the errors Leggett et al. (1996) quote for the temperatures, their data

could easily accommodate a transformation which contains changes in slope that exactly compensate for the temperature differences between the model and data. Thus we cannot formally rule out the possibility that unsampled features in our temperature scale have produced artifacts in the mass-radius relationship.

However, when we substitute the better-sampled temperature transformation of Bessell (1995), the changes in the mass-radius relation remain. To straighten the mass-radius relation, we would need a color-temperature transformation like that plotted in Figure 5. For reference, Figure 5 also shows the Bessell (1995) transformation and our fit to the Leggett et al. (1996). data. Obviously, the features required to bring the data into correspondence with the models would be difficult to hide within the Bessell transformation, but not impossible, especially if the atmospheric models used to measure the temperatures introduce additional errors. Nonetheless, neither the models nor the measurements offer any evidence for the existence of abrupt features in the color-temperature transformation; to suppress the changes in the mass-radius relation we would have to invoke them arbitrarily.

2.4.2. The Models

Finally, we will consider whether the differences between the theoretical and observed mass-radius relationship can be accommodated by uncertainties in the theoretical models. In Figure 6, we plot mass-radius relations for a wider variety of models. Like the mass-radius relation of Baraffe & Chabrier (1996), they are all relatively straight; none show the features we observe in the 8 parsec sample. It is possible that their straight appearance is due to a fundamental and unalterable property of low-mass stars. If this is true, and can be demonstrated, it will be very useful. It will provide valuable constraints on the transformations we have used, and might significantly improve our knowledge of the (mass, M_V) relation, and consequently the mass function of the lower main sequence.

More likely, the similarity of the mass-radius relations are due to common simplifications employed by the models that produce them. For low-mass fully-convective and almost fully-convective model stars, the radiative region at the surface establishes the thermal equilibrium configuration, and thereby the nuclear energy generation rate (see Cox & Giuli 1968). Hence the luminosities of these models are extremely sensitive to the surface boundary conditions. However, changes in the surface boundary conditions affect the luminosity almost exclusively through changes in the effective temperature, rather than in radius.

Dorman, Nelson & Chau (1989) illustrate this last point by considering the effect of

modifying the surface opacities. An increase in opacity results in a decrease in the surface temperature, because the optical depth rises more steeply with pressure ($dP/d\tau \sim g/\kappa$) and our line of sight cannot penetrate to as high a temperature as it did before. This drop in temperature will lower the luminosity of the model star unless it expands to compensate. But even a small expansion will radically change the nuclear reaction rates in the core, because of their sensitive dependence on the central temperature. Consequently, the net effect of the increased opacity is an appreciably lower effective temperature and luminosity, but only a slightly larger radius. It is for this reason that model subdwarfs have higher temperatures and luminosities, but essentially the same radii as model dwarfs of equivalent mass (see Schwarzschild 1958).

This insensitivity of model radius to surface physics is not confined to opacities alone. The steepening of the main sequence between $-1.8 < \log(L/L_{\odot}) < -1.5$ exhibited by all of the models shown in Figure 2 was first calculated by Copeland, Jensen, & Jorgensen (1970) by including the effects of H_2 molecules on the envelope equation-of-state. The presence of an H_2 dissociation region near the model surface decreases the adiabatic gradient, making the star appear hotter and more luminous than it would otherwise. Figure 3 of Copeland et al. (1970) shows that their models including this effect are displaced along lines of almost constant radius from those which neglect it.

These examples illustrate the weak dependence of radius on changes in the surface physics. For a low-mass, fully-convective model star, the radius is sensitive primarily to the interior composition, equation-of-state, and the nuclear reaction rates. We can see this more clearly by considering the classic study of Hayashi & Hoshi (1961), and Hayashi (1961). They showed that for fully convective, and therefore isentropic, models, the quantity,

$$E = 4\pi(\frac{\mu}{N_A k})^{5/2} G^{3/2} K M^{1/2} R^{3/2}, \tag{5}$$

has a constant value of 45.48. In this equation, μ is the mean molecular weight, N_A is Avogadro's number, k is Boltzmann's constant, G is the gravitational constant, and K is the coefficient of the polytropic law which represents these stars:

$$P = KT^{5/2}. \tag{6}$$

Models of fully-convective pre-main sequence stars of fixed M shrink to smaller radius at roughly constant temperature until they reach an equilibrium between luminosity and nuclear generation rate. Thus the final radius depends on the internal structure. An alternative way to see this is to recognize that K and μ in equation 5 depend primarily on interior properties, and R must adjust to their values such that $E = 45.48$.

While published models have explored carefully the changes in the surface physics for models of different mass, they have not explored the limits allowed by changes in interior

structure or physics that might occur with mass. These are possible if, for example, stars develop gradients in μ due to diffusion or nuclear burning. [2] In this case we might expect the fully convective stars to be homogeneous, and the higher mass stars with radiative cores to sustain a μ gradient. The boundary between models with convective cores and models that are fully convective is 0.3 $M_{\odot}$, coincident with the change in slope of the mass-radius relation of Figure 3. If models do not properly account for changes in interior composition above and below this mass, it might help explain the discrepancy with the observations.

Another possibility is that the non-ideal corrections to the interior equation-of-state, which become large at low masses, might change the slope of the mass-radius relation. An extreme example of non-ideal effects was suggested for the sun by Pollock & Alder (1978) who, in an attempt to resolve the solar neutrino problem, proposed that iron might be immiscible with hydrogen in the solar interior. Later calculations by Alder, Pollock, & Hansen (1980) and Iyetomi & Ichimaru (1986), showed that the temperature in the solar core is about three times hotter than the critical point in their phase diagrams, so separation should not occur there. However, comparison of their phase diagrams for an iron-hydrogen plasma to the run of temperature and pressure in low-mass stellar models plotted by Dorman et al. (1989) shows that the conditions they calculate for phase separation are present near the center of stars between 0.1 and 0.2 $M_{\odot}$.

The point of this discussion is not to suggest that any one of these examples is responsible for the discrepancy between the models and observations, but rather to suggest that the limits to our knowledge inevitably translate into uncertainties in the radii of our stellar models. It is important to know the size of these uncertainties, because even small changes in the mass-radius relationship can significantly affect the orbital period evolution of cataclysmic variables.

3. The Cataclysmic Variable Orbital Period Distribution

The downward jump in the main sequence we have presented, and the change in the mass-radius relation it implies, bear an obvious relevance to the orbital period evolution of cataclysmic variables. In order to maintain the mass transfer which characterizes the cataclysmic variables, the secondaries in these binaries must fill their Roche lobes. This condition immediately establishes a relation between the mean density of the secondaries and the orbital period (Faulkner, Flannery and Warner 1972; Eggleton 1983)— a relation

[2] Similar changes might result if the nuclear reaction rates change radically in their dependence on temperature or density— a possibility we mention only for completeness.

which is essentially independent of the mass of the accreting white dwarf (as long as it is the more massive component). Consequently, the mass-radius relationship of the secondary uniquely fixes the orbital period of a cataclysmic binary. As the binary evolves, and the secondary loses mass, changes in the slope of the mass-radius relationship, inasmuch as they affect the way the secondary responds to mass loss, will change the way in which the orbital period evolves.

Theoretical investigations of cataclysmic variable evolution (Paczynski 1967; Faulkner 1971; Vila, 1971; Rappaport, Joss, & Webbink 1982; McDermott & Taam 1989; Hameury 1991, and many more) generally rely upon theoretical models of the secondary star to provide the mass-radius relationship. As we have seen, the theoretical mass-radius relationships are all essentially featureless between 0.6 and 0.1 $M_{\odot}$. In contrast to this approach, we will explore the effects of the observationally derived mass-radius relationship upon the evolution of cataclysmic variables. We will show that the mass-radius relation we have constructed implies that cataclysmic variables in the orbital period range 3.5 to 2.0 hours must either evolve more quickly, or transfer mass more slowly, than binaries above and below this range. This result derives from the steeper slope of the observed mass-radius relation between 0.3 and 0.16 $M_{\odot}$; a small reduction in mass results in a larger shrinkage in radius, and therefore a larger reduction in orbital period.

The critical assumption in this approach is that the mass-radius relation measured for single stars can be applied to the mass-losing secondaries in cataclysmic variables. This is equivalent to assuming that the secondary remains in thermal equilibrium in spite of the effects of mass-loss and irradiation. There are sound reasons, both observational and theoretical, to suppose that this is true for at least some of the cataclysmic variables. We will discuss these reasons before presenting the results of our study.

Beyond the assumption of thermal equilibrium, the results of this section depend only upon the observed mass-radius relationship, the size of Roche equipotentials, and Kepler's third law. They do not depend upon theoretical models of low-mass stars, nor upon the theoretical discussions of the previous section. The ultimate promise of the investigation we present is to establish a better observational link between low-mass stars and cataclysmic variables, thereby increasing the number of useful observational constraints on low-mass stellar models.

3.1. The Assumption of Thermal Equilibrium

Observationally, there is evidence that at least some, and maybe most, cataclysmic variables secondaries have radii like normal main sequence stars (Webbink 1990; Ritter 1980; Marsh 1990; Wade & Horne 1988). Webbink (1990) constructed an empirical mass-radius relationship for 24 eclipsing cataclysmic binaries and found it to be a good match to the theoretical models. He has kindly provided his results in tabular form (Webbink 1997) for comparison to our mass-radius relationship. As Figure 7 shows, his measurements are in excellent agreement with the mass-radius relationship of the 8 parsec sample. Clearly the effects of mass loss have not drastically increased the radii of the secondaries in these systems, but the data do not exclude small effects that might have significant consequences for our results. Consequently, we will also discuss theoretical issues concerning the assumption of thermal equilibrium.

Intuitively, we expect that mass loss from the secondary will cause it to have a radius larger than a main sequence star of equivalent mass if the mass is removed faster than the star can adjust its equilibrium structure. Hence, when the mass loss timescale, defined as $M_2/\dot{M}_2$, drops below the Kelvin-Helmholtz timescale, the assumption of thermal equilibrium may become invalid. For a secondary in a cataclysmic variable with an orbital period of 3 hours, the Kelvin-Helmholtz timescale is 2.4×10^8 yr, which yields a limiting mass loss rate of $1.3 \times 10^{-9} M_\odot$/yr. For rates higher than this, the main sequence mass-radius relation may no longer apply.

Warner (1995) presents a calibration of average mass transfer rates in cataclysmic variables versus the absolute magnitudes of their disks (his Figure 9.8, see also Smak 1989,1994). This relationship suggests that the dwarf novae have average mass transfer rates near or below this limit. Thus we may expect our application of the mass-radius relation for single stars to apply to some, if not all, cataclysmic variables. This conclusion is dependent upon the degree to which it is valid to infer mass transfer rates from the brightness of accretion disks (Smak 1994). It also assumes that there have been no recent episodes of much higher mass-transfer that might have temporarily driven the the secondary out of thermal equilibrium.

Another effect that might cause the secondary to have a radius larger than a single star of equivalent mass is irradiation. The effects of irradiation by the companion and disks are similar to other changes in the surface boundary condition of stellar models (Tout et al. 1989). As we discussed in section 2.4, the surface boundary condition affects primarily the temperature of the models, not the radius. Thus we intuitively expect irradiation to have large effects on the temperature of secondaries in cataclysmic variables, but little effect on radii. This intuition is borne out by detailed models (Podsiadlowsky 1991;Hameury

et al. 1993) up until the incident flux is roughly equal to the emergent flux. Above this, the radius increases rapidly with increasing irradiation. Expected values for the maximum incident flux on secondaries in dwarf novae with periods longer than 3 hours fall below the emergent flux, except perhaps during outburst (Warner 1995), suggesting that the effects of irradiation do not invalidate our application of the mass-radius relation for single stars to dwarf novae secondaries.

Considered together, the observational and theoretical evidence suggests that we might expect the results of the exploration we present in the following section to apply to those cataclysmic variables which maintain modest mass-transfer rates typical of the dwarf nova subclass. Those systems with brighter disks and higher inferred mass transfer rates may contain secondaries larger than implied by our mass-radius relationship. These will still feel the effects of the mass-radius relationship, but it will be convolved with the effects of their departure from thermal equilibrium. We will not attempt to account for these effects in this paper.

3.2. The Orbital Period Histogram

In Figure 8 we show the histogram of orbital periods for non-magnetic cataclysmic variables with known periods. This plot is reproduced from Warner (1995). For further details see also the tabulation by Ritter & Kolb (1995). In order to sustain mass transfer most cataclysmic variables must lose angular momentum, either through the emission of gravitational radiation (Kraft, Matthews, & Greenstein 1962) or via some other mechanism, and thereby evolve to shorter orbital period. Thus, while the distribution of periods at which cataclysmic variables are born certainly affects the period histogram, any attempt to fully explain it must account for period evolution.

At least one feature of the distribution, the minimum period, has been accounted for on this basis. Paczynski (1967) and Faulkner (1971) recognized that at very low mass, the mass-losing secondary must become degenerate, and expand in response to mass loss. This corresponds to a change in the sign of slope of the theoretical mass-radius relation. The effect of this change is to drive the orbital period back to longer values. Paczynski & Sienkiewicz (1983) and Rappaport et al. (1982) have examined the dependence of the minimum orbital period on a variety of physical parameters. These are important explorations, because they connect the observations of cataclysmic variables to the internal physics and composition of the stellar models in a fundamental way.

Attempts to explain the other most obvious feature, the shortage of systems with

orbital periods between 2 and 3 hours, are more problematic. Most explanations derive from a suggestion of Robinson et al. (1981), who proposed that some mechanism causes secondaries to shrink below their Roche lobes at a mass of 0.3 $M_{\odot}$, stopping the mass transfer until shrinkage of the orbit re-establishes it at shorter period. In the interim, the binaries do not appear as cataclysmic variables, and the gap is explained. They noted that 0.3 $\mathrm{M}_{\odot}$ is the mass below which models are fully convective and speculated that the onset of convection in the core might induce the secondary to shrink. D'Antona & Mazzitelli (1982) found a theoretical basis to expect such shrinkage in the sudden mixing of ^{3}He when the star becomes fully convective, but later calculations by McDermott and Taam (1989) showed this effect to be negligible.

Most recent models for explaining the period gap (Rappaport, Verbunt, & Joss 1983; Spruit & Ritter 1983; Hameury et al. 1988; McDermott & Taam 1989) invoke an *ad hoc* "disruption" in the angular momentum loss, which temporarily separates the secondary from its Roche lobe. Because the main angular momentum loss mechanism is believed to be magnetic braking, this disruption requires a decrease in either the stellar wind or the magnetic field of the secondary, presumed to be associated with the onset of convection in the core of the secondary. While there are plausibility arguments for a disruption of this sort in the magnetic braking (see Taam & Spruit 1989), there is no theory which predicts them, and no convincing observational evidence that they occur. On the contrary, observations of low-mass stars in the Pleiades and Hyades by Jones, Fischer, & Stauffer (1996) show no evidence for the reduction of braking in stars below 0.3 $M_{\odot}$. For these reasons, the disrupted braking models are somewhat unsatisfying. They also preclude applying the information contained in observations of the period gap to improve structural models of low-mass stars; the measurements are used up in constraining free parameters of the disrupted braking model.

The disrupted braking models all require that secondaries of systems with periods just longer than 3 hours be out of thermal equilibrium due to mass transfer. This is so that a disruption in the mass transfer at an orbital period of 3 hours will cause the secondary to shrink within its Roche lobe, and remain there until the orbital period evolves through the gap. As we have discussed, it is not clear whether all cataclysmic variables meet this requirement.

The mass-radius relationship we have presented offers the possibility to improve upon the disrupted braking models. We will explore this possibility in the next section, first by showing that the features in the mass-radius relation correspond to periods associated with the period gap, and then describing the simple way in which they affect the orbital period distribution of cataclysmic variables.

3.3. Orbital Periods and the Mass-Radius Relation

The motivation for this investigation derives from a match we noted between the M_V of the main sequence feature fitted by Reid & Gizis (1997), and the M_V of cataclysmic variable secondaries at the long end of the period gap as quantified by Warner (1995). Warner (1995) presented a plot of the absolute magnitudes of cataclysmic variable secondaries versus the logarithm of their orbital periods (his Figure 2.56). From a linear fit to the data he derived:

$$M_V = 16.7 - 1.1\ \log P_{orb}(\mathrm{h}). \tag{7}$$

Using this equation, the secondary of a cataclysmic variable with a 3 hour orbit should be $M_V = 11.4$. From the fit of Reid & Gizis (1997) to the 8 parsec data (equation 1), the downturn in the color-magnitude diagram starts at $M_V = 11.6$.

This correspondence in M_V between the step in the main sequence and the period gap suggests that we test for a direct connection in the mass-radius plane. To get orbital periods for a secondary of given mass and radius requires the use of a formula for the volume-radius of the Roche lobe. From Eggleton (1983), we have:

$$\frac{R_L}{a} = \frac{0.49q^{2/3}}{0.6q^{2/3} + \ln(1 + \mathrm{q}^{1/3})}, \tag{8}$$

where a is the orbital separation, and q is the ratio of the primary to the secondary mass (M_2/M_1). We can apply our measured mass-radius relation to cataclysmic secondaries through equation 8 by requiring that the radius of the secondary R_2 be fixed by its mass, M_2, according to the mass-radius relation we have measured. Under the condition for mass transfer, $R_L = R_2$, equation 8 then yields the orbital separation. Using this, along with Kepler's third law,

$$P_{orb} = \left[\frac{4\pi^2 a^3}{G(M_1 + M_2)}\right]^{1/2}, \tag{9}$$

we get the orbital period. The result is insensitive to q as long as $q < 1$. We have used a constant mass for the primary, $M_1 = 0.8M_\odot$, in the examples which follow.

Figure 9 shows the mass-radius relation of the Reid & Gizis (1997) fit to the 8 parsec sample we calculated in section 2. For comparison, we have included mass-radius relations which result from using theoretical mass-magnitude relations of Kroupa et al. (1993) and Chabrier et al. (1996) along with the empirical one of Henry & McCarthy (1993). When applied to cataclysmic variables, these relations become evolutionary tracks. The mass-losing secondaries will evolve down the mass-radius relation until their structure starts to diverge from that of single stars. We can calculate their period at each point using

equations 8 and 9. Furthermore, equations 8 and 9 together yield the well-known mean density relationship:

$$P_{orb}(\mathrm{h}) \approx 8.75 \left(\frac{\mathrm{M}}{\mathrm{R}^3}\right)^{-1/2} \tag{10}$$

(Faulkner, Flannery and Warner 1972; Eggleton 1983), where M and R are now in solar units.

Using equation 10, we have plotted lines of equal orbital period on Figure 9 to illustrate the effect of changes in the slope of the mass-radius relationship. Between the points labeled 1 and 2, the slow shrinkage of the secondary in response to mass loss causes the orbital period to decrease very slowly. Between 2 and 3, the orbital period changes more rapidly for the same amount of mass loss. This change in the rate of orbital period evolution generates the period gap in our model.

We can quantify the mechanism illustrated in Figure 9 by introducing the formula for total orbital angular momentum,

$$J = \frac{M_1 M_2}{M_1 + M_2} a^2 \frac{2\pi}{P_{orb}}, \tag{11}$$

and assuming that angular momentum is lost from the binary at a constant rate, $\dot{J} = c$. This assumption is certainly wrong, but will serve to illustrate how the period gap arises. The time spent between points 1 and 2 is given by:

$$t_{1,2} = \frac{J_2 - J_1}{\dot{J}}, \tag{12}$$

and likewise for the time between points 2 and 3. Inserting the appropriate values for P_{orb} (3.47, 3.41 and 2.02 h) and J (2.35, 1.54, and 0.68 $\times 10^{51}$ g-cm^2/s), the ratio of the times $t_{1,2}/t_{2,3} = 0.94$, independent of c. Thus a binary containing a lobe-filling secondary that obeys the mass-radius relation in Figure 9 takes almost as long to evolve from 3.47 to 3.41 h as it does from 3.41 to 2.02. This has important implications for the orbital period distribution of cataclysmic variables. Under the simplest assumption of constant cataclysmic variable birth rate, there should be 22 times as many binaries in the bin between 3.47 and 3.41 h as there are in equal size bins at shorter period (above 2.02 hours).

It is also important to consider what happens to the rate of mass loss from the secondary under these assumptions. We can calculate this using:

$$\dot{M}_{2;1,2} = \frac{M_{2;2} - M_{2;1}}{t_{1,2}} \tag{13}$$

Where M_2 refers to the secondary, and the later subscripts refer to the labeled points in Figure 9. We find that the mass loss rate for the secondary is slightly higher between

1 and 2 than it is between 2 and 3 ($\dot{M}_{2;1,2}/\dot{M}_{2;2,3} = 1.13$). So not only does the binary spend less time between 2 and 3, the mass transfer rate there is also lower. Since either effect might contribute to a decrease in the observed number of cataclysmic variables between $P_{orb} = 3.41$ and 2.02 h, the change in the slope of the mass-radius relation at 0.3 $M_\odot$ provides a general qualitative reason to expect a reduction in the observed numbers of cataclysmic variables between 3.41 and 2.02 h. In the next section, we will introduce the more realistic assumption that angular momentum loss decreases slowly with time, as enforced by a prescription for magnetic braking.

3.4. An Illustration Using Magnetic Braking

The contents of this section are meant as an illustration only. Many of the results are highly sensitive to the exact slope of the measured mass-radius relation, which is not well-constrained due to observational noise. Nonetheless, the results illustrate the general shape of the orbital period distribution and mass loss rates implied by the mass-radius relation, using more sophisticated assumptions than in the previous section. If the model for the period gap we present survives continued scrutiny, the sensitivity of the the results in this section to the mass-radius relation will eventually be beneficial. It will allow even crude measurements of cataclysmic variable properties to constrain low-mass stellar models.

Our calculations in this section are based on the formulae of the previous section, but with a finer spacing in mass. From these formulae we have calculated sample orbital period distributions and mass transfer rates using a parameterized angular momentum loss rule of the form,

$$\dot{J} = -3.8 \times 10^{-30}\ M R_\odot^4 \left(\frac{R}{R_\odot}\right)^\gamma \left(\frac{2\pi}{P_{orb}}\right)^3 \text{ dyn} - \text{cm}, \tag{14}$$

following Rappaport et al. (1983), who rely upon Verbunt & Zwaan (1981). We do *not* introduce artificial reductions in this loss, as required for most models of the period gap. Consequently, our models include angular momentum loss in excess of the rate caused by gravitational radiation, even below the period gap. This is in better agreement with the observations of accretion disk magnitudes below the period gap, which frequently require mass transfer rates too high to be driven by gravitational radiation alone (Warner 1995).

Figure 10 shows the results of calculations using the mass-radius relation we constructed from the Reid & Gizis (1997) fit to the 8 parsec data, and the empirical (mass, M_V) relation of Henry & McCarthy (1993). This relation is the dotted line in Figures 3, 4 and 9. We used the angular momentum loss parameterization of equation 14 with $\gamma = 4$ and included gravitational radiation loss according to Landau & Lifschitz (1958). We fixed the mass

of the white dwarf primary at 0.8 $M_{\odot}$, equivalent to assuming all the transferred mass is eventually lost from the system. Calculations using conservative transfer yield almost identical results.

The top panel of Figure 10 shows the time spent at each orbital period, from equation 12. These times have been normalized to equal orbital period intervals to allow direct comparison to the orbital period histogram (bottom panel). Under the assumption of uniform cataclysmic variable birthrate (with initial periods above 5 hours), this curve represents the space density of cataclysmic variables at each orbital period. We calculated curves using the other two mass-radius relations in Figure 9, with similar results. The curve based on the Kroupa et al. (1993) (mass, M_V) relation gives a broader and shorter peak at 3.5 h, but still has small values at longer period, while the Chabrier et al. (1996) based relation yields a larger peak at 3.5 h. If there were no selection effects involved in the discovery of cataclysmic variables, these curves would not be promising; the bump near 3.5 h is too narrow, and values for longer period are too low to match the observed orbital period histogram.

However, the middle panel of Figure 10 shows the secondary mass loss rate as a function of orbital period, from equation 13. The increase in the mass loss near 3.5 h is a real effect of the change in slope of the mass-radius relation. The subsequent drop is no more rapid than before, but is compressed on this plot because of the long time spent by the model in the vicinity of $P_{orb} = 3.5$ h. Because higher mass transfer rates result in brighter disks, and increase the likelihood of detection, the middle curve in Figure 10 represents an important factor in the discovery probability for cataclysmic variables. Obviously, the higher mass transfer rates at long period can compensate, to some degree, for the shortage in our model space densities in the same portion of the upper panel. The degree of compensation is impossible to calculate without precise knowledge of cataclysmic variable discovery selection effects. Considered together, the panels in Figure 10 suggest that the mass-radius relation we have constructed can account for the main features of the cataclysmic variable orbital period distribution.

4. Summary and Conclusions

We have shown that the color-magnitude diagram of the lower main sequence exhibits a feature which is apparently associated with changes in the slope of the mass-radius relation for low-mass stars. Investigations in the mass-radius plane show that the locations of the interesting features correspond roughly to the boundaries of the known cataclysmic variable orbital period gap. This correspondence relies upon the best available empirical

data: the observed color magnitude of the 8 parsec sample from Reid & Gizis (1997), the bolometric corrections of Leggett (1995), the mass-visual magnitude relation of Henry & McCarthy, and the measured orbital periods of cataclysmic variables (Warner 1995; Ritter & Kolb 1995).

By introducing additional theoretical assumptions, chiefly regarding the structural similarity of low-mass single stars and cataclysmic variable secondaries, we find that the observed mass-radius relation can generate a period gap similar to the one observed. Unlike disrupted braking models, this explanation does not require any *ad hoc* adjustments to the angular momentum loss from the binary. It also does not demand that all secondaries above the period gap be out of thermal equilibrium, a requirement of disrupted braking models that is in conflict with the observations. Furthermore, the explanation we have uncovered allows angular momentum loss below the period gap in excess of that caused by gravitational radiation, in better agreement with the observations (Warner 1995).

Our explanation does not apply directly to systems with high mass transfer rates, which may have secondaries larger than single stars of equivalent mass. These systems will still be affected by changes in the mass-radius relation, but in ways that are complicated by the fact that the secondaries are not necessarily in thermal equilibrium. We have not attempted to unravel these effects in this paper.

Our investigation suggests two further lines of inquiry, the first of which is completely theoretical. Given the uncertainties in the transformations we have applied to the data, it is possible that the changes in the mass-radius relation are artifactual. If it is possible to show theoretically that slope changes such as those we observe in the mass-radius relation are disallowed, we will be forced to abandon any further pursuit of their relationship to cataclysmic variables and attribute the connection explored in this paper to an appealing, but accidental, coincidence. However, theoretical investigations of this sort would have another important use, arising from constraints they would provide on the combined color-temperature and mass-magnitude relations. These might improve the reliability of investigations of the initial mass function and the luminosity function of low-mass stars.

The second course to pursue is observational: primarily, to improve the measurements of the mass-radius relationship. There is a notable shortage of fundamental mass-radius measurements, acquired from eclipsing binaries where the masses and radii are both directly measurable. The only system available below 0.5 $M_\odot$ is CM Dra, and there is evidence that this system may be metal poor (Metcalfe et al. 1996; Gizis 1997). It is possible that the eclipsing cataclysmic variables themselves may contribute to this effort. If independent arguments can establish that cataclysmic variable secondaries follow a normal main sequence mass-radius relationship, the data from Webbink presented in Figure 7 offer an

order of magnitude increase in the number of direct empirical mass-radius determinations.

Finally, if the results of this paper are correct, there are extensive numerical experiments to conduct. Hameury (1991) has emphasized the value of cataclysmic variables for testing low-mass stellar models; cataclysmic variable properties are highly sensitive to the physics governing the secondary stars. If future investigations can use the information provided by the size and location of the period gap, without introducing *ad hoc* components to the theory, it will be a valuable addition to the very few measurables offered by single stars. Since much of the physics governing stellar interiors is inaccessible by any other means, it is important to explore every observational constraint our ingenuity can devise.

5. Acknowledgments

We are indebted to the referee R. Webbink, who provided us his data on masses and radii of cataclysmic variable secondaries. His comments resulted in substantial improvements to this paper, both in content and presentation.

This work was begun with support from NASA through grant number HF-01041.01-93A from the Space Telescope Science Institute, which is operated by the Association of Universities for Research in Astronomy, Inc., under NASA contract NAS5-26555; it was completed with the generous support of the Sherman Fairchild Foundation. INR acknowledges partial support from NASA through grant GO-05913.01-94A. JEG gratefully acknowledges partial support from both a Greenstein Fellowship and a Kingsley Fellowship. MSO'B receives support from a GAANN fellowship, through grant number P200A10522 from the Department of Education.

REFERENCES

Alder, B. J., Pollock, E. L., & Hansen, J. P. 1980, Proc. Natl. Acad. Sci. USA, 77, 6272

Alexander, D. R., & Ferguson, J. W. 1994, ApJ, 437, 879

Allard, F., & Hauschildt, P. H. 1995, ApJ, 445, 433

Baraffe, I., & Chabrier, G. 1996, ApJ, 461, L51

Baraffe, I., Chabrier, G., Allard, F., & Hauschildt, P. H. 1995, ApJ, 446, L35

Bessell, M. S. 1995, in Proc. ESO Astrophys. Symp., The Bottom End of the Main Sequence and Beyond, ed. Chris Tinney (Berlin:Springer), 123

Brett, J. M. 1995, A&A, 295, 736

Chabrier, G., Baraffe, I., & Plez, B. 1996, ApJ, 459, L91

Copeland, H., Jensen, J. O., & Jorgensen, H. E. 1970, A&A, 5, 12

Cox, J. P., & Giuli, R. T. 1968, Principles of Stellar Structure (New York:Gordon and Breach), vol. 2, 738

D'Antona, F., & Mazzitelli, I. 1982, ApJ, 260, 722

D'Antona, F., & Mazzitelli, I. 1994, ApJS, 90, 467

D'Antona, F., & Mazzitelli, I. 1996, ApJ, 456, 329

Dorman, B., Nelson, L. A., & Chau, W. Y. 1989, ApJ, 342, 1003

Eggleton, P. P. 1983, ApJ, 268, 368

European Space Agency 1997, The Hipparcos Catalogue, ESA SP-1200

Faulkner, J. 1971, ApJ, 170, L99

Faulkner, J., Flannery, B. P., & Warner, B. 1972, ApJ, 175, L79

Gizis, J. E. 1997, AJ, 113, 806

Gliese, W., & Jahreiss, H. 1991, Preliminary Version of the Third Catalogue of Nearby Stars, (CNS3)

Fontaine, G., Graboske, H. C., Jr., & Van Horn, H. M. 1977, ApJS, 35, 293

Hameury, J.-M. 1991, A&A, 243, 419

Hameury, J.-M., King, A. R., Lasota, J.-P., & Raison, F. 1993, A&A, 277, 81

Hameury, J.-M., King, A. R., Lasota, J.-P., & Ritter, H. 1988, MNRAS, 231, 535

Hawley, S. L., Gizis, J. E., & Reid, I. N. 1996, AJ, 112, 2799

Hayashi, C. 1961, PASJ, 13, 450

Hayashi, C., & Hoshi, R. 1961, PASJ, 13, 442

Henry, T. J., & McCarthy, D. W. 1993, AJ, 106, 773

Hoxie, D. T. 1973, A&A, 26, 437

Iyetomi, H., & Ichimaru, S. 1986, Phys. Rev. A, 34, 3203

Jones, B. F., Fischer, D. A., & Stauffer, J. R. 1996, AJ, 112, 1562

Kraft, R. P., Matthews, J., & Greenstein, J. L. 1962, ApJ, 136, 312

Kroupa, P., Tout, C. A., & Gilmore, G. 1993, MNRAS, 262, 545

Landau, L. & Lifschitz, E. 1958, The Classical Theory of Fields (Oxford: Pergammon)

Leggett, S. K., Allard, F., Berriman, G., Dahn, C. C., & Hauschildt, P. H. 1996, ApJS, 104, 117

Leggett, S. K., Harris, H. C., & Dahn, C. C. 1994, AJ, 108, 944

Marsh, T. R. 1990 ApJ, 357, 621

Metcalfe, T. S., Mathieu, R. D., Latham, D. W., & Torres, G. 1996, ApJ, 456, 356

McDermott, P. N., & Taam, R. E. 1989, ApJ, 342, 1019

Monet, D. G., Dahn, C. C., Vrba, F. J., Harris, H. C., Pier, J. R., Luginbuhl, C. B., & Ables, H. D. 1992, AJ, 103, 638

Neece, G. D. 1984, ApJ, 277, 738

Paczynski, B. 1967, Acta Astr., 17, 287

Paczynski, B., & Sienkiewicz, R. 1983, ApJ, 268, 825

Patterson, J. 1984, ApJS, 54, 443

Podsiadlowski, Ph. 1991, Nature, 350, 136

Pollock, E. L., & Alder, B. J. 1978, Nature, 275, 41

Popper, D. M. 1980, ARA&A, 18, 115

Rappaport, S., Joss, P. C., & Webbink, R. F. 1982, ApJ, 254, 616

Rappaport, S., Verbunt, F., & Joss, P. 1983, ApJ, 275, 713

Reid, I. N., & Gizis, J. E. 1997, AJ, in press

Reid, I. N., Hawley, S. L., & Gizis, J. E. 1995, AJ, 110, 1838

Ritter, H. 1980, The Messenger, 21, 16

Ritter, H., & Kolb, U. 1995, in X-ray Binaries, ed. W. H. G. Lewin, J. van Paradijs, & E. P. J. van den Heuvel (Cambridge:Cambridge University Press), 578

Robinson, E. L., Barker, E. S., Cochran, A. L., Cochran, W. D., & Nather, R. E. 1981, ApJ, 251, 611

Saumon, D., Chabrier, G., & Van Horn, H. M. 1995, ApJS, 99, 713

Schwarzschild, M. 1958, Structure and Evolution of the Stars, (New York: Dover), 140

Smak, J. 1989, Acta Astr., 39, 317

Smak, J. 1994, Acta Astr., 44, 45

Spruit, H. C., & Ritter, H. 1983, A&A, 124, 267

Taam, R. E., & Spruit, H. C. 1989, ApJ, 345, 972

Tout, C. A., Eggleton, P. P., Fabian, A. C., & Pringle, J. E. 1989, MNRAS, 238, 427

Tout, C. A., Pols, O. R., Eggleton, P. P., & Han, Z. 1996, MNRAS, 281, 257

Verbunt, F., & Zwaan, C. 1981, A&A, 100, L7

Vila, S. C. 1971, ApJ, 168, 217

von Hippel, T., Gilmore, G., Tanvir, T., Robinson, D., & Jones, D. H. P. 1996, AJ, 112, 192

Wade, R. A., & Horne, K. 1988, ApJ, 324, 411

Warner, B. 1995, Cataclysmic Variable Stars (Cambridge:Cambridge University Press)

Webbink, R. F. 1990, in Accretion-Powered Compact Binaries, ed. C. W. Mauche (Cambridge:Cambridge University Press), 177

Webbink, R. F. 1997, private communication

FIGURE CAPTIONS

Fig. 1.— Color magnitude diagrams for stars in the 8 parsec sample of Reid & Gizis (1997). Open circles indicate data expected to have larger photometric errors (see text). The lower panel shows the same data as in the upper left, but incorporating better distances from Hipparcos, where available.

Fig. 2.— Comparison between the observations and theoretical models. Both panels show M_V, $(V-I)$ measurements from the 8 parsec sample, transformed into $\log(L/L_\odot)$ using data from Leggett et al. (1996) (*filled and open circles*), and the fit of Reid & Gizis (1997) (*dotted line*). Theoretical models are divided between the plots as follows: *upper squares*: Dorman et al. (1989) with the Fontaine, Graboske, & Van Horn (1977) equation-of-state; *upper triangles*: D'Antona & Mazzitelli (1994); *upper pentagons*: Neece (1984); *lower squares*: Baraffe & Chabrier (1996); *lower triangles*: Baraffe et al. (1995).

Fig. 3.— Mass-radius relation for the M_V, $(V-I)$ 8 parsec data (*open and filled circles*) and for the models of Baraffe & Chabrier (1996)(*solid line*). Masses are from the (mass, M_V) relation of Henry & McCarthy (1993). The *dotted line* is the fit of Reid & Gizis (1997) transformed in the same manner as the data. See the text for a discussion of the error bars.

Fig. 4.— Mass-radius relation of the M_K, $(I-K)$ 8 parsec data (*open and filled circles*), and the data tabulated by Popper (1980) (*filled squares*). For reference, the M_V, $(V-I)$ fit of Reid & Gizis (1997) (*dotted line*) remains as in Figure 4. The eclipsing, spectroscopic binaries YY Gem and CM Dra are marked. For the latter we have plotted the newer masses and radii from Metcalfe et al. (1996)

Fig. 5.— The color-temperature transformation (*filled circles*) that would be required to bring the observational data into exact correspondence with the models of Baraffe & Chabrier (1996). The transformations of Bessell (1995)(*solid line*) and our fit to Leggett et al. (1996)(*dotted line*) are shown for reference.

Fig. 6.— Mass-radius relations for a variety of models. They are: *solid line*: Baraffe & Chabrier (1996); *dotted line*: Tout et al. (1996); *short dashes*: D'Antona & Mazitelli (1994); *long dashes*: Dorman et al. (1984); *dot-short dashes*: Neece (1984)

Fig. 7.— The mass-radius relation of eclipsing cataclysmic variables from Webbink (1990; 1997)(*large circles*). For comparison, the *small circles* are the mass-radius relation for the 8 parsec sample shown previously in Figure 3. The fit of Reid & Gizis (1997)(*dotted line*) and the models of Baraffe & Chabrier (1996)(*solid line*) are also plotted as in Figure 3.

Fig. 8.— The orbital period distribution of non-magnetic cataclysmic variables. Adapted from Warner (1995).

Fig. 9.— The mass-radius relation and its application to cataclysmic variable secondaries. The curves are the transformed fit of Reid & Gizis (1997) with masses from the (mass, M_V) relations of: *dotted line*: Henry & McCarthy (1993); *dashed line*: Kroupa et al. (1993); and *dot-dash*: Chabrier et al. (1996). The solid lines are lines of constant orbital period from equation 10. See the text for discussion of the points labelled 1, 2 and 3.

Fig. 10.— Orbital period and mass-loss evolution calculated from the observed mass-radius relation. *Top Panel*: Time spent between orbital periods normalized by the period interval (see equation 12). *Middle panel*: secondary mass loss rate (see equation 13). *Bottom panel*: Orbital period histogram for all non-magnetic cataclysmic variables (*solid line*), and for dwarf novae only (*filled regions*).

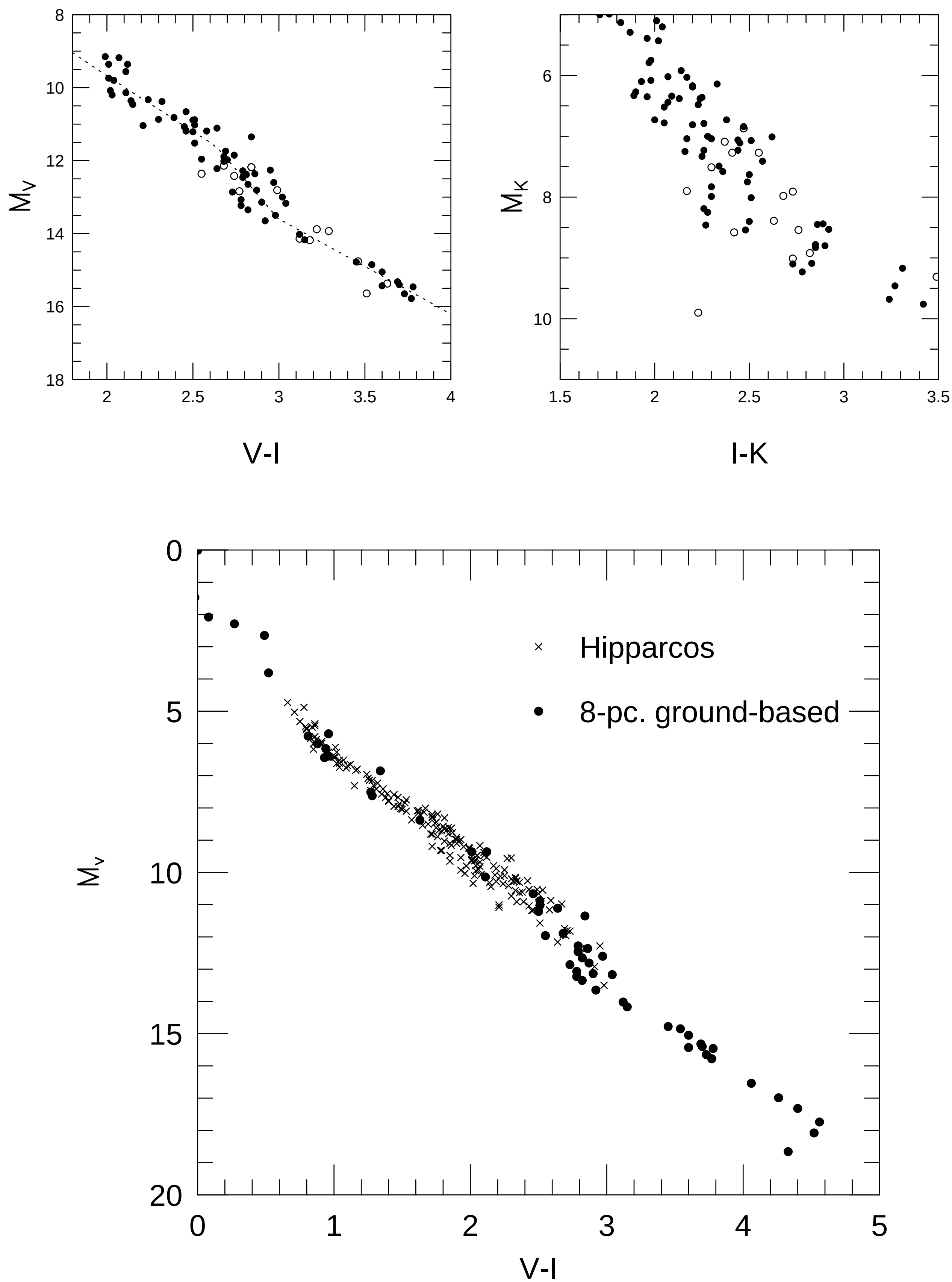
M_V
V-I
M_K
I-K
Hipparcos
8-pc. ground-based

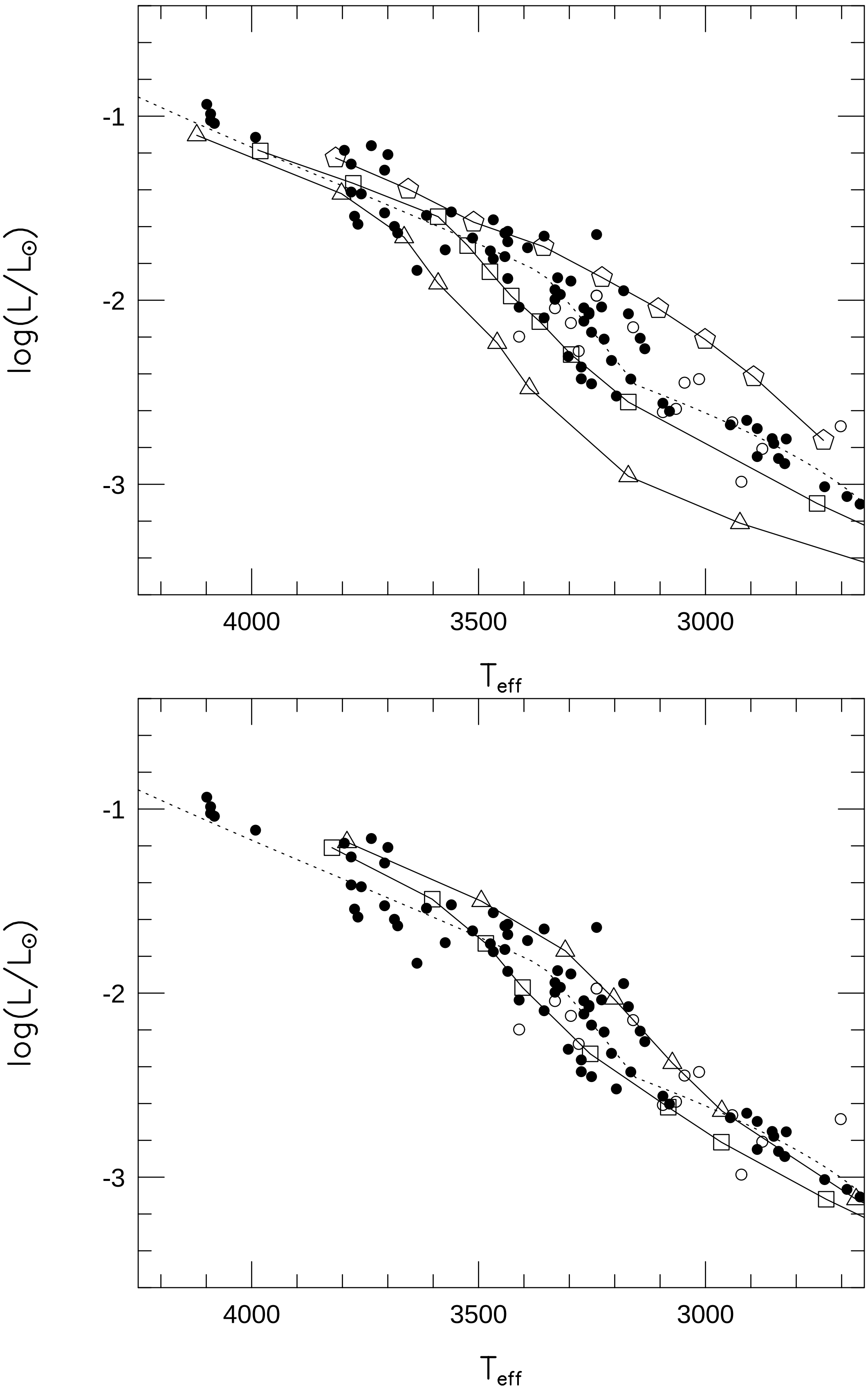

log(L/L⊙)
-1
-2
-3
4000
3500
3000
T_eff
log(L/L⊙)
-1
-2
-3
4000
3500
3000
T_eff

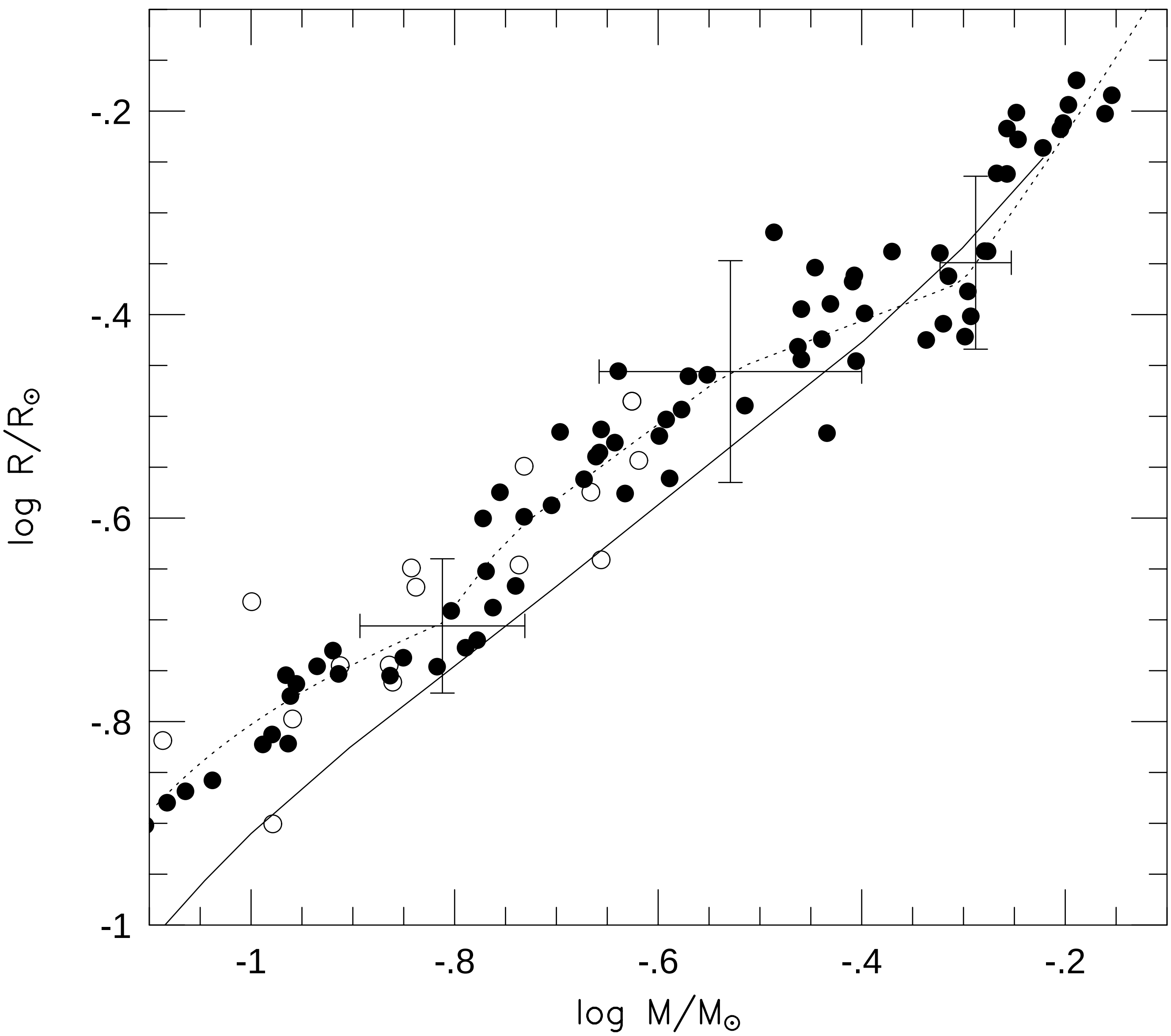

-.2
-.4
-.6
-.8
-1
log R/R⊙
-1
-.8
-.6
-.4
-.2
log M/M⊙

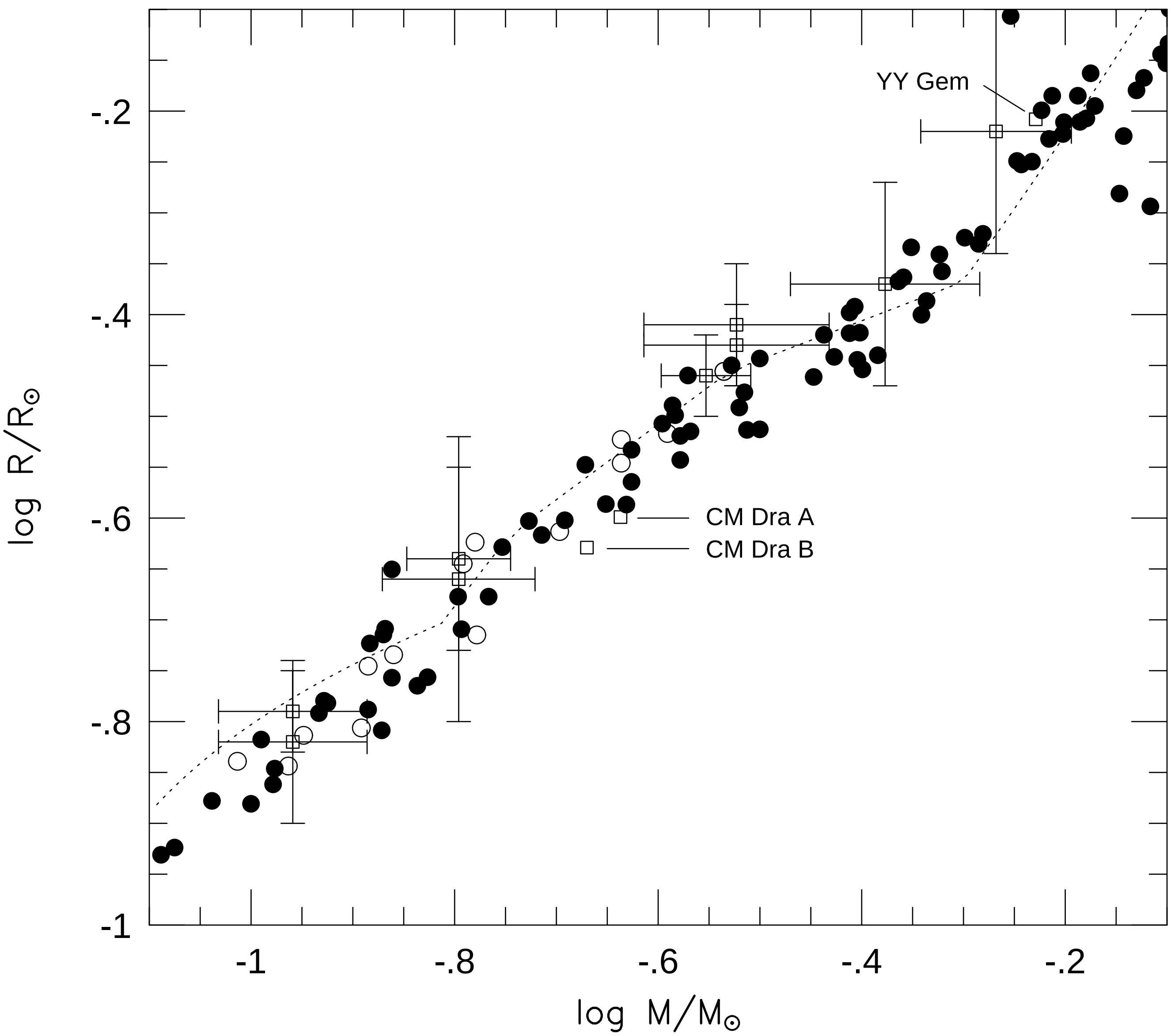

YY Gem
CM Dra A
CM Dra B
log R/R$_\odot$
log M/M$_\odot$
-.2
-.4
-.6
-.8
-1
-1
-.8
-.6
-.4
-.2

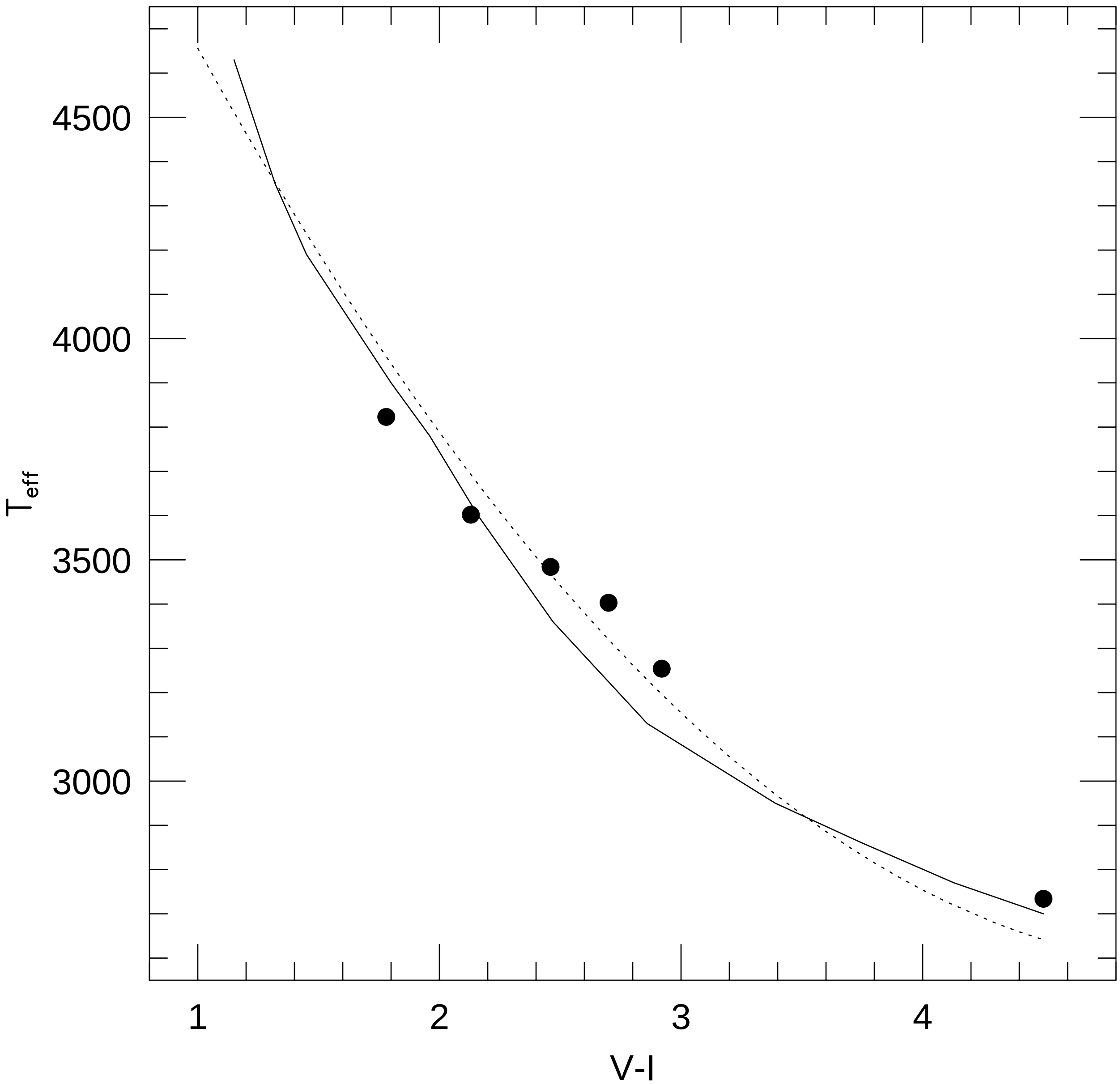
4500
4000
3500
3000
T_{eff}
1
2
3
4
V-I

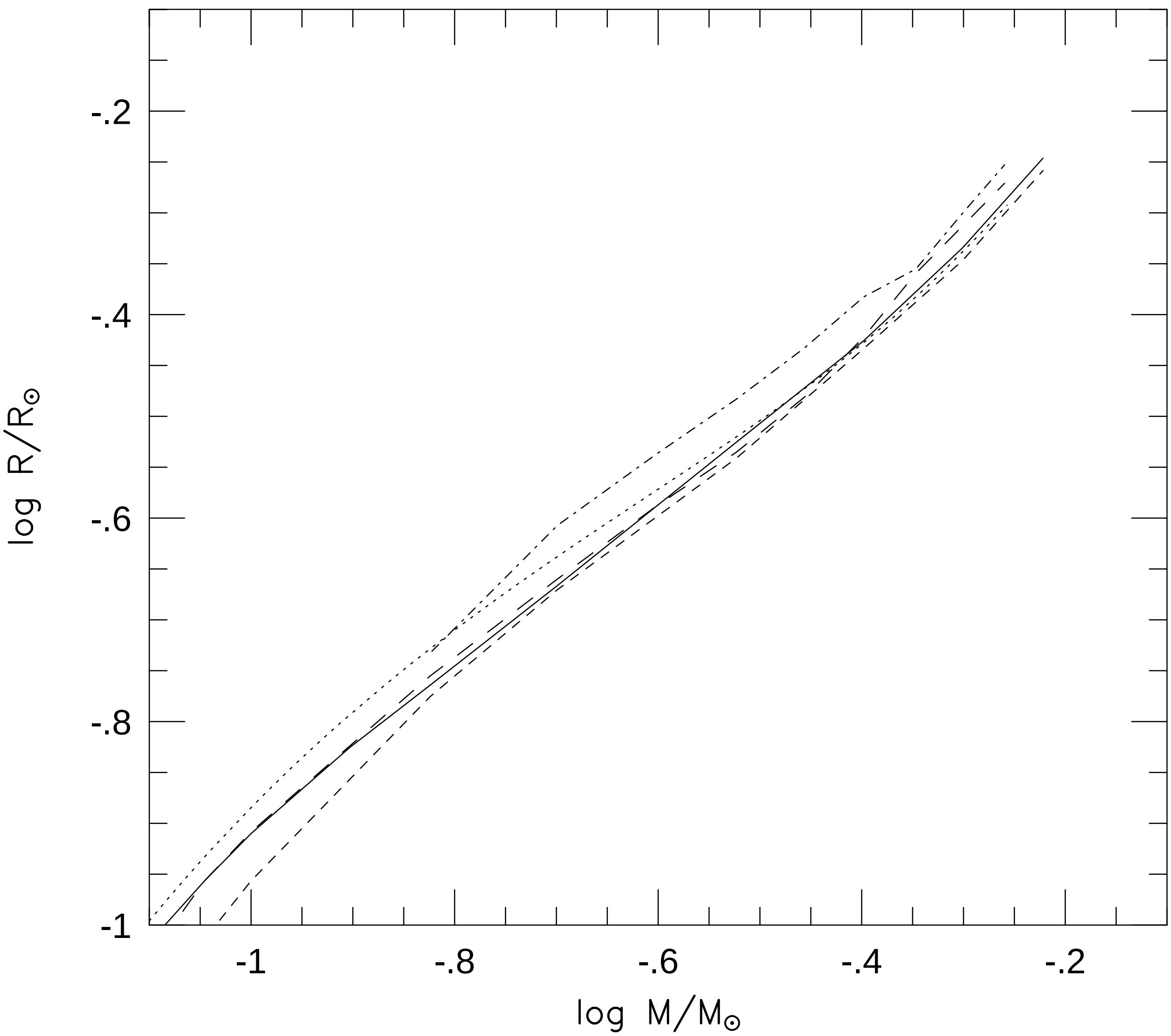

-.2
-.4
-.6
-.8
-1
log R/R⊙
-1
-.8
-.6
-.4
-.2
log M/M⊙

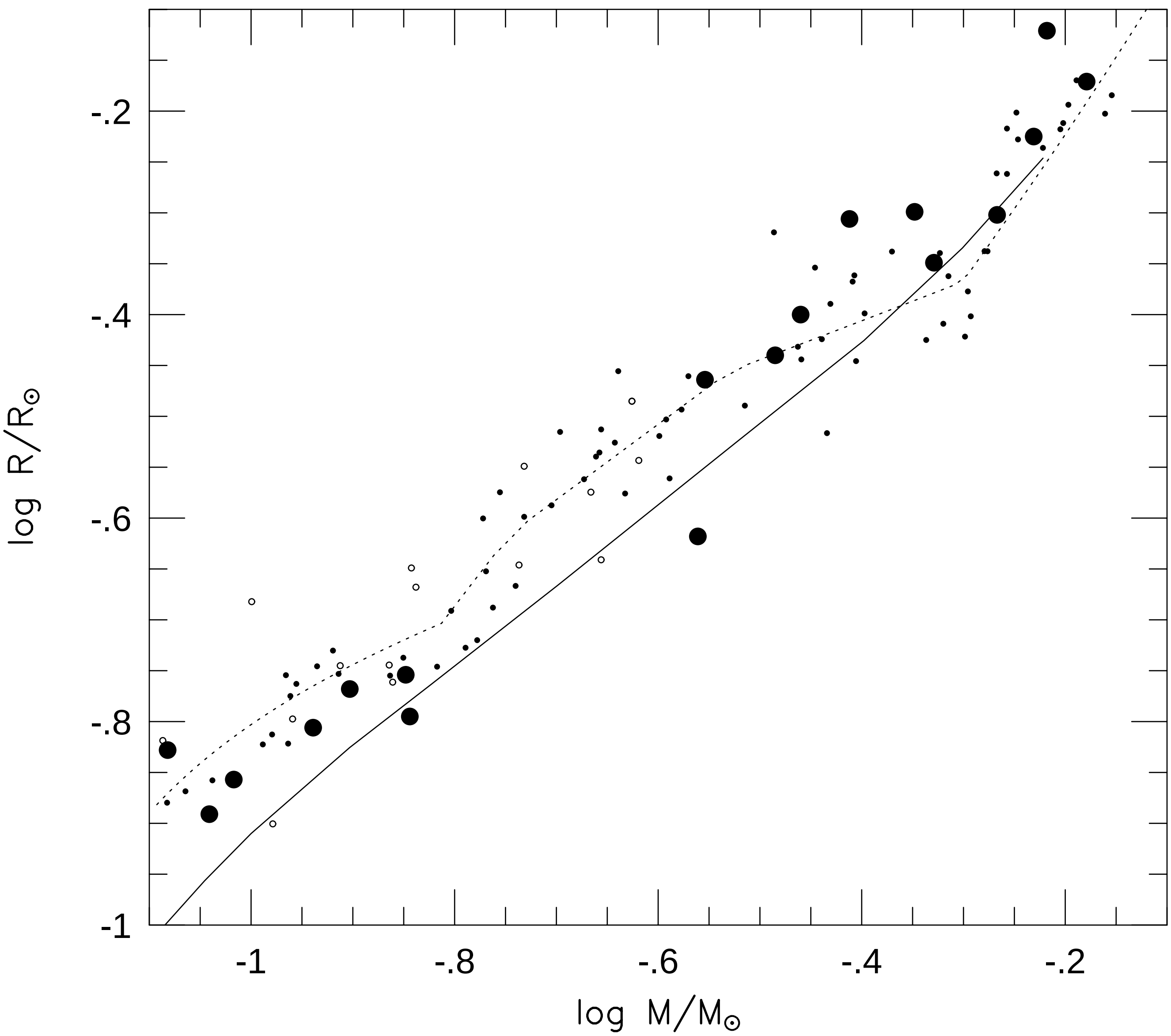

-.2
-.4
-.6
-.8
-1
log R/R☉
-1
-.8
-.6
-.4
-.2
log M/M☉

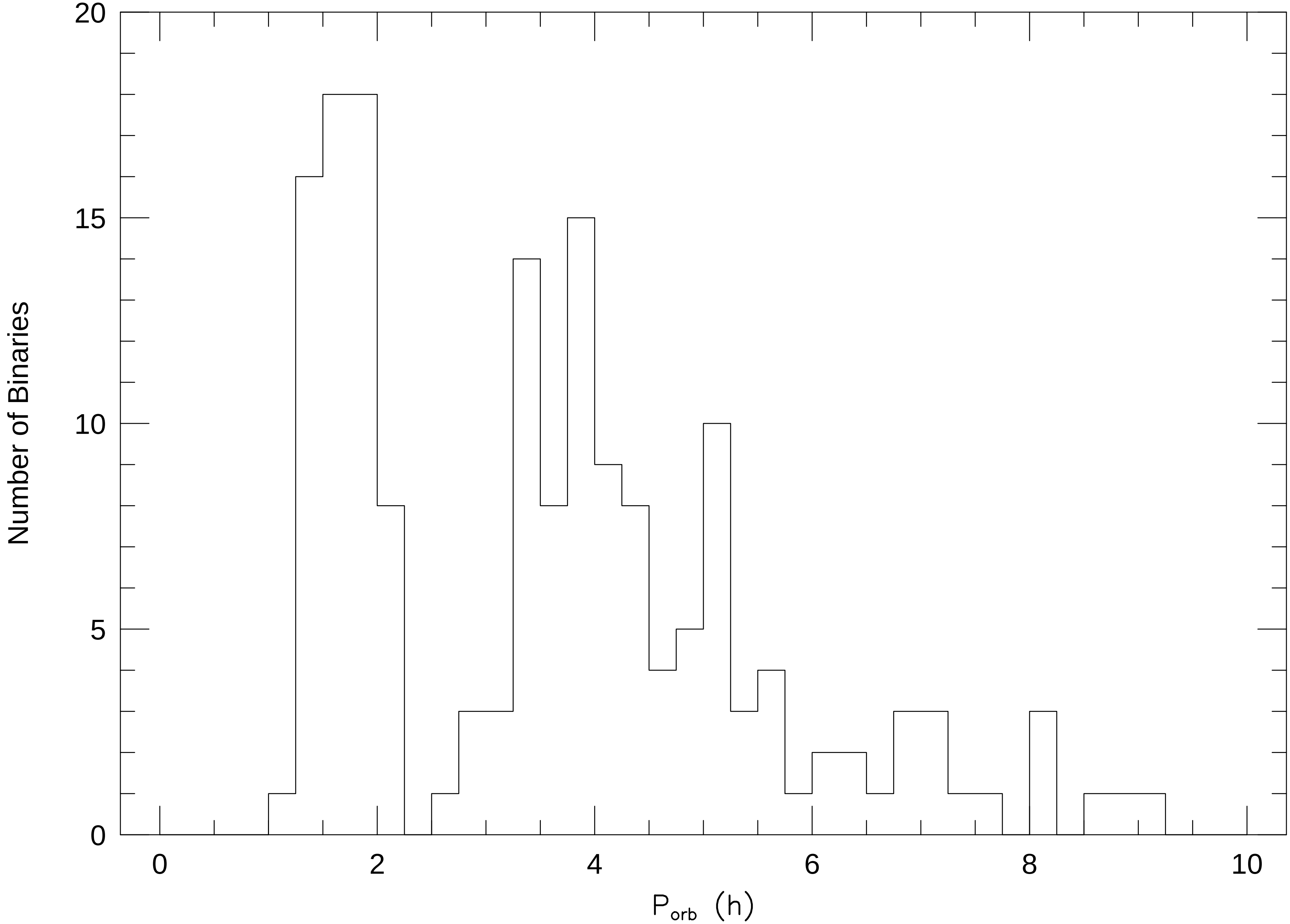

20
15
10
5
0
Number of Binaries
0
2
4
6
8
10
P_{orb} (h)

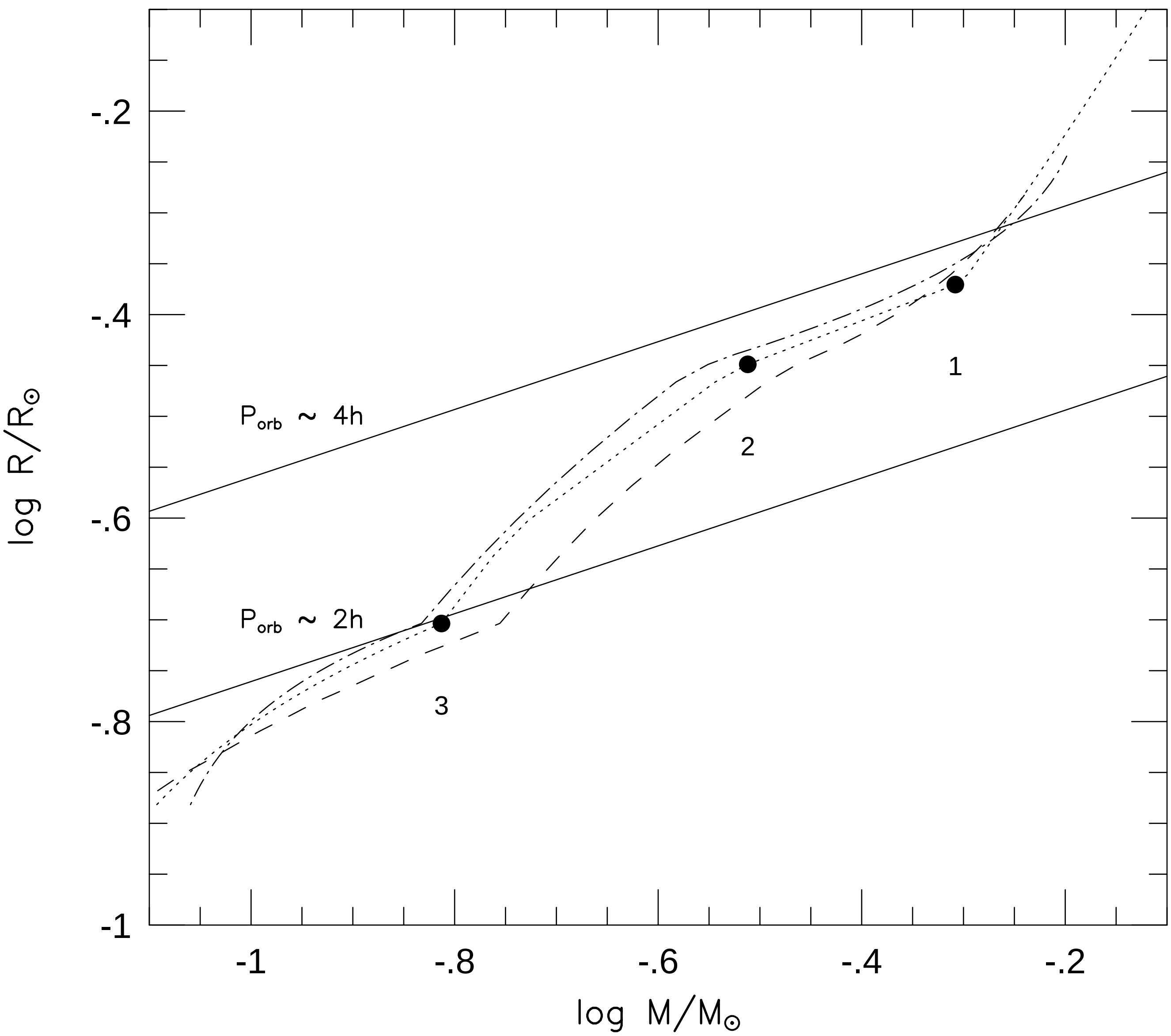

-.2
-.4
-.6
-.8
-1
-1
-.8
-.6
-.4
-.2
log R/R⊙
log M/M⊙
P orb ~ 4h
P orb ~ 2h
1
2
3

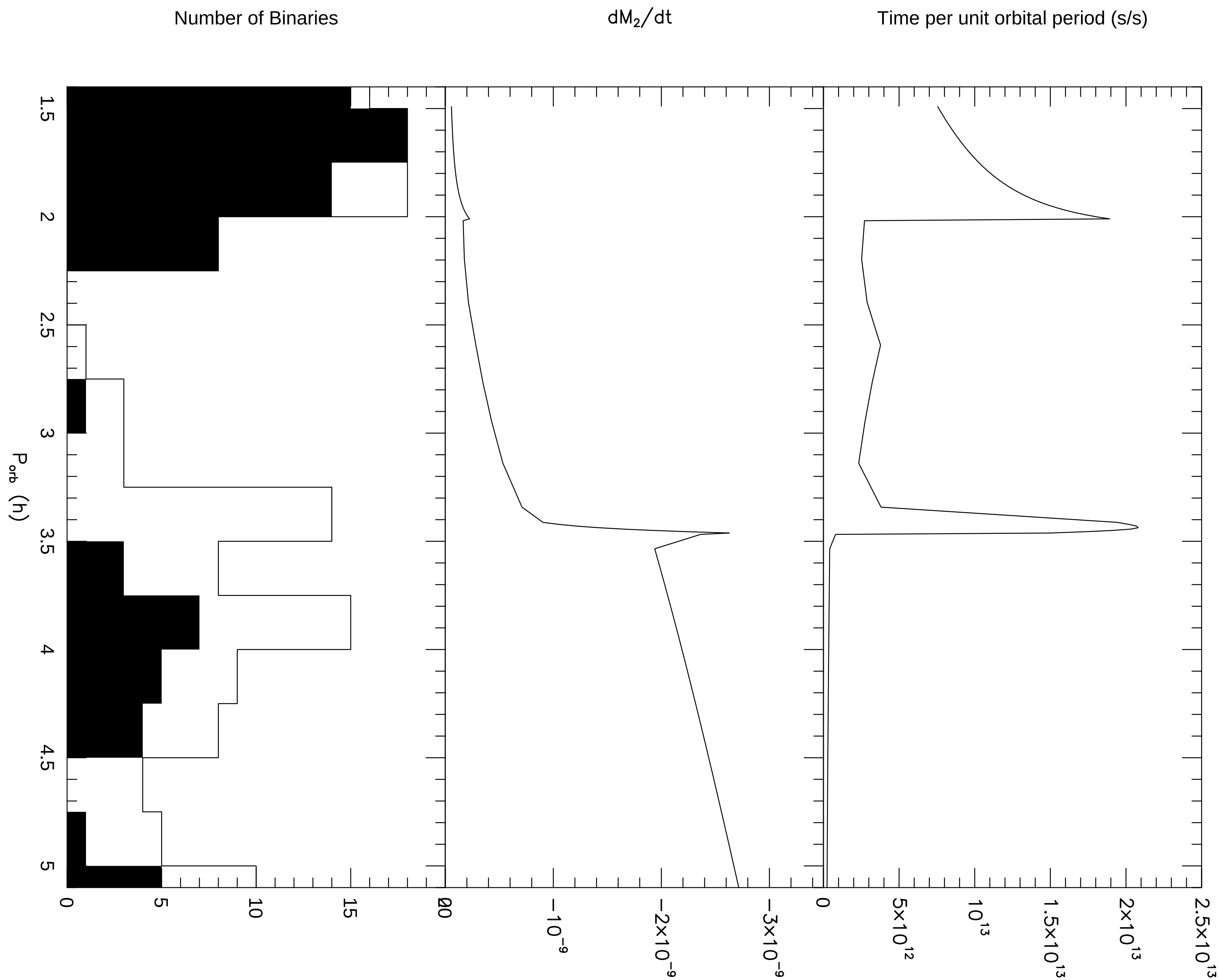

Number of Binaries
dM2/dt
Time per unit orbital period (s/s)
Porb (h)
1.5
2
2.5
3
3.5
4
4.5
5
0
5
10
15
20
0
−10−9
−2×10−9
−3×10−9
0
5×1012
1013
1.5×1013
2×1013
2.5×1013